Scientific Reports

https://doi.org/10.1038/s41598-026-47430-9

Article in Press

Revisiting the application of variable infiltration capacity (VIC) model in the Colorado River Basin using SMAP and GRACE

Received: 19 November 2025

Accepted: 31 March 2026

Published online: 03 April 2026

Cite this article as: Wang Z., Ghimire S., Whitney K.M. *et al.* Revisiting the application of variable infiltration capacity (VIC) model in the Colorado River Basin using SMAP and GRACE. *Sci Rep* (2026). https://doi.org/10.1038/s41598-026-47430-9

Zhaocheng Wang, Swastik Ghimire, Kristen M. Whitney, Giuseppe Mascaro, Mu Xiao, Haowen Yue & Enrique R. Vivoni

Revisiting the Application of Variable Infiltration Capacity (VIC) Model in the Colorado River Basin using SMAP and GRACE

Zhaocheng Wang[1,2], Swastik Ghimire[1,2], Kristen M. Whitney[3,4], Giuseppe Mascaro[1,2], Mu Xiao[5], Haowen Yue[1,2], and Enrique R. Vivoni[1,2,*]

[1]School of Sustainable Engineering and the Built Environment, Arizona State University, Tempe, AZ, USA.

[2]Center for Hydrologic Innovations, Arizona State University, Tempe, AZ, USA.

[3]NASA Goddard Space Flight Center, Greenbelt, MD, USA.

[4]Earth System Science Interdisciplinary Center, University of Maryland, College Park, MD, USA.

[5]Scripps Institution of Oceanography, University of California, La Jolla, CA, USA.

Revised for *Scientific Reports*
March 30, 2026
Submission ID f2a4f5dc-057e-433e-9b57-6f4612640d1c

* *Corresponding author address:* Enrique R. Vivoni, WCPH, Room 418, 777 E. University Drive, Arizona State University, Tempe, AZ, 85287-8704, tel: 480-727-3575, fax: 480-965-8102, email: vivoni@asu.edu.

Abstract

The Colorado River Basin (CRB) is a crucial water supply source experiencing prolonged drought conditions. Hydrologic models of the CRB have historically relied on streamflow calibration alone, limiting confidence in their representation of spatially distributed hydrologic processes. Here, we implemented a calibration and multi-source evaluation framework for the Variable Infiltration Capacity (VIC) model using observations from ground snow stations, streamflow records, and NASA's Soil Moisture Active Passive (SMAP) and Gravity Recovery and Climate Experiment (GRACE) missions. After model calibration with snow and streamflow records, VIC achieved an excellent streamflow performance at key sub-basin outlets in the CRB (e.g., Nash-Sutcliffe Efficiency of 0.96 in the Upper Basin). Independent evaluations with SMAP further revealed a strong model performance in reproducing surface (R^2 = 0.71) and root-zone (R^2 = 0.81) soil moisture, with systematic elevation-dependent patterns in the comparison. A multi-year evaluation with GRACE demonstrated a robust reproduction of basin-scale terrestrial water storage dynamics and their interannual variability (R^2= 0.66–0.86). This multi-source evaluation framework establishes the VIC model capacity to represent subsurface water storage dynamics in different land cover types, providing enhanced confidence for supporting water management in the CRB.

Keywords: land surface modeling, satellite remote sensing, snow, soil moisture, terrestrial water storage anomalies, spatial patterns.

Introduction

The Colorado River Basin (CRB) sustains 40 million population across seven U.S. states and Mexico, providing critical water resources for municipal supply, irrigated agriculture, hydroelectric power generation, and recreational activites[1]. Since 2000, the CRB has experienced the Millennium Drought, a period characterized by rising temperatures, reduced precipitation, declining snowpacks, and consequently diminished inflows into reservoirs[2–5]. Over successive dry years, the streamflow efficiency has declined as soil moisture and groundwater have been progressively depleted, reflecting a process of aridification[6–8]. Increasing water demands further widened the imbalance between renewable water supply and consumptive uses, which includes evaporative losses from reservoirs[1,9]. These compounding stressors have depleted storage in Lakes Mead and Powell to unprecedented levels below 30% of their total capacity, triggering the first-ever U.S. federal shortage declarations and their associated water curtailments in the CRB[10]. As the basin approaches the expiration of its operational guidelines in 2026, robust modeling frameworks that are grounded in hydrologic processes and constrained by Earth observations are essential to inform interstate negotiations and develop long-term adaptation strategies[11–13].

Process-based hydrologic models are central to quantifying natural streamflow and characterizing basin responses to climate variability and change[14,15]. Among these, the Variable Infiltration Capacity (VIC) model has

been one of the most consulted hydrologic model in the CRB (Fig. 1) for sensitivity analyses[16–18], seasonal forecasting[19], and future projections[20,21]. Since its release in 1994, VIC has a long record of continuous model development, including advances in land surface physics, snow representation, vegetation parameterization, and meteorological forcings[22–26]. Model outputs from VIC have been used by the U.S. Bureau of Reclamation (USBR) to generate naturalized streamflow (Q), defined as streamflow reconstructed to represent conditions without the effects of human activities such as reservoir regulation, diversions, and consumptive water use, which is subsequently used in the Colorado River Simulation System, the core water resources systems model that supports operational decision-making and planning across water agencies in the CRB[1].

Despite this extensive use, most VIC applications in the CRB remain predominantly calibrated against streamflow data at a limited number of stations[20,27]. This limited observational constraint, while sufficient for reproducing outflow, fails to adequately test the simulations of internal hydrologic variables and the hydrologic partitioning that governs streamflow efficiency. Consequently, models achieving reasonable streamflow performance may exhibit divergent representations of critical hydrologic processes including snow accumulation, infiltration rates, soil moisture dynamics, and subsurface water changes. Recent investigations have demonstrated the value of integrating satellite-based Earth observations as independent benchmarks for evaluating hydrologic model

performance[28–32]. For example, evaluation of VIC model outputs with Moderate Resolution Imaging Spectroradiometer (MODIS) land surface temperature and snow cover fraction products enabled spatially distributed diagnostics of internal model behavior, revealing systematic biases in meteorological forcings[33]. The procedure implemented by Xiao *et al.* (2018)[33] improved the representation of snow process in the CRB beyond what could be achieved through streamflow-only calibration at a few basin outlets.

Beyond optical remote sensing, observations from microwave and gravimetric satellite missions provide independent observations of water storage or its changes, which are important for the description of drought propagation from meteorological to streamflow conditions[34]. The Soil Moisture Active Passive (SMAP) mission, operational since 2015, provides surface (0–5 cm) soil moisture (*SM*) observations and root-zone (0–100 cm) soil moisture estimates at 9-km spatial resolution, providing a more comprehensive drought detection capability as compared to meteorological indices that neglect antecedent water storage conditions[35–37]. Estimates of root-zone soil moisture are derived through assimilation of SMAP surface observations into the NASA Catchment Land Surface Model (CLSM). The Gravity Recovery and Climate Experiment (GRACE) and its successor GRACE Follow-On measure integrated terrestrial water storage anomalies (*TWSA*) through gravity field observations. When combined with independent estimates of snow, soil moisture, and surface water storage,

GRACE observations have been used to infer groundwater losses during the Millennium Drought in the CRB[6,38,39]. Collectively, SMAP and GRACE observations provide complementary benchmarks on water storage dynamics, with SMAP characterizing soil moisture variability at high temporal frequency and kilometer-scale spatial resolution, and GRACE capturing low-frequency, basin-scale variations in vertically integrated terrestrial water storage changes that include deeper subsurface and groundwater components, which are valuable for hydrologic model evaluations[40,41].

This study revisits the VIC model application in the CRB with the objective of strengthening confidence in its representation of spatially distributed hydrologic processes and water storage dynamics under prolonged drought conditions. We integrated high-resolution meteorological forcings, recalibrating sub-basin parameters relative to previous VIC applications[16–21, 27, 33, 57], and evaluating the model against multiple, independent Earth observation products (Fig. 1). While streamflow observations at a limited number of gauging stations are used for calibration, this approach contrasts with previous VIC efforts in the CRB by extending model evaluation to include spatially distributed diagnostics of soil moisture and terrestrial water storage changes using independent Earth observation datasets. By incorporating Earth observations of subsurface water changes, the evaluation framework directly tests the VIC representation of water storage dynamics, which are critical for water

resource planning under prolonged drought conditions. Results show that VIC captures the spatiotemporal patterns of anomalies in soil moisture and terrestrial water storage changes across the CRB. These findings establish a comprehensive, satellite observation-constrained framework based on the VIC model for seasonal forecasting and long-term water resource planning in the CRB, as these applications depend on the accurate representation of basin-scale water storage dynamics.

Results and Discussion

CRB Hydroclimate from VIC Modeling Outputs. After updating the forcing datasets and performing the model recalibration (see Methods), VIC simulations reproduced well the snow-dominated hydroclimate regime, including the seasonal timing and interannual variability of streamflow as well as the spatial distribution of streamflow generation across major sub-basins and elevation bands (Figs. 2 and S1). VIC simulated streamflow (Q, sum of runoff and baseflow) exhibits close agreement with naturalized streamflow records in the Upper Colorado River Basin (UCRB), with Nash-Sutcliffe Efficiency (NSE) of 0.96, Pearson correlation coefficient (CC) of 0.98, and a systematic bias of 0.01 $km^3\ yr^{-1}$ across 1984–2023 (Fig. 2a). In the UCRB, precipitation (P) is primarily partitioned into snowfall during the cool season (October–March), which accumulates as seasonal snowpacks in high-elevation areas. The subsequent release of this water storage through snowmelt, combined with spring precipitation, leads to a pronounced and sustained discharge during April–July that accounts for more than 60% of

annual Q[42,43]. This four-month period is also critical for operational predictions of reservoir operations in the CRB. In late-summer season, rainfall contributes minimally to basin-scale total streamflow generation, as it is largely consumed by evapotranspiration (ET)[44]. Model performance is further demonstrated through analyses of two major water-producing sub-basins, the Green and Upper Colorado (Fig. 2b–c), which collectively generate about 83% of total UCRB streamflow. Model performance is lower in the Lower Colorado River Basin (LCRB; NSE = 0.65), reflecting its arid climate and limited runoff generation. However, since the UCRB contributes more than 90% of the streamflow in the CRB, VIC accurately represents basin-wide streamflow variability.

The spatial distribution of snowpack conditions and streamflow generation further show the model performance in representing the hydrologic dependence on elevation in the CRB. The mean annual SWE (Fig. 2d) shows that snow accumulation is concentrated in the northern, high-elevation headwaters, while the mean annual Q (Fig. 2e) shows a concentration of discharge in those same topographic domains. Fig. 2f presents the cumulative contribution curves of mean annual SWE and Q as a function of fractional contributing area (A_f) by sorting cells from high to low elevation, with the basin hypsometry shown on the right axis. These curves quantify the spatial variability in the CRB, by showing that ~85% of both SWE and Q originate from only ~18% of the basin area situated above 2,000 m. Below this elevation threshold, SWE exhibits a steeper decline rate

with elevation than *Q*, reflecting a transition from persistent snowpacks to intermittent snow regimes[45,46]. These spatial diagnostics and the calibration with point data demonstrate that VIC reproduces plausible spatial hydrologic patterns in the CRB (see Methods).

Evaluation of VIC Model Performance Against Earth Observations. *SM* is a critical variable for model evaluation as it regulates the partitioning of *P* into *ET*, *Q*, and subsurface water storage changes[47–49]. Fig. 3a–b demonstrates that VIC simulated standardized anomalies in *SM* exhibit a strong agreement with SMAP L4 products over the full monthly time series from 2015 to 2024, yielding coefficients of determination (R^2) of 0.71 for the surface layer (0–10 cm), and 0.81 for the root-zone (0–100 cm) averaged in the CRB. For comparison with SMAP root-zone soil moisture (0–100 cm), VIC soil moisture from layers 1 and 2 was aggregated and, where the combined depth exceeded 100 cm, proportionally scaled to represent an effective 0–100 cm soil column. In the surface layer, VIC and SMAP track closely during the *SM* accumulation phase, with *z*-scores rising from near-zero values in October to their peak wetness of +0.5 to +1.0 standard deviations in February to March. Lower surface *SM* agreement emerges during the spring depletion period (April–July) when SMAP consistently shows *z*-scores ~0.2 to 0.4 standard deviations higher than VIC, indicating that SMAP retains wetter surface conditions during the main streamflow season. This pattern is consistent across most years, except in 2021 when SMAP surface *SM* was lower than VIC. In the late-summer period, VIC *SM*

exceeds SMAP and has reduced temporal variability, a pattern seen in all years.

The root-zone *SM* dynamics (Fig. 3b) exhibit attenuated seasonal amplitude compared to the surface layer, with lower peak *z*-score in the accumulation phase and a longer accumulation period. This leads to a temporal lag in peak *SM* timing between the surface and root-zone layers, reflecting the vertical water redistribution in the soil column. Root-zone *SM* agreement between VIC and SMAP remains robust throughout the complete annual cycle, with mean *z*-score differences consistently below 0.2 standard deviations. Notably, a temporal offset of approximately one month emerges during the March through July transition period, with VIC root-zone moisture peaks occurring later than corresponding SMAP maxima.

Temporal correlation maps (Fig. 3c–d) reveal spatial differences in the agreement between VIC and SMAP, exhibiting a systematic elevation dependence. For both surface and root-zone layers, the highest correlations ($CC > 0.7$) occur in elevations below 2,000 m, whereas the lowest correlations ($CC < 0.5$) are in high-elevation regions (see insets for elevation dependence of *CC*). Based on this performance, elevation-band analysis was conducted (Fig. S2), revealing that the mismatch in high-elevation root-zone values stem from a systematic offset in time. Specifically, in the 2000–3000 m elevation band, VIC root-zone *SM* peaks in late May while SMAP peaks in April. A similar one-month offset persists in the 3000–4000 m band, though both products show similar seasonal

amplitudes and overall temporal evolutions. Since *SM* typically peaks upon snow disappearance in snow-covered regions[45], the delayed timing in VIC likely reflects field conditions. This is confirmed by quantitative in-situ evidence from SNOTEL stations (Fig. S3), which shows that across both mid- (2000–3000 m) and high-elevation (3000–4000 m) bands, root-zone *SM* peaks in late May and June, respectively. In both cases, the VIC simulations and SNOTEL observations coincide, while the SMAP maximum consistently occurs one month earlier (April and May, respectively). Differences in root-zone *SM* between VIC and SMAP in high elevation regions can arise from two distinct sources. First, uncertainties related to the SMAP Level-4 product reflect its intrinsic structural characteristics, as the root-zone SM is derived through assimilation of surface observations into CLSM using a fixed 100 cm soil column and model-dependent vertical redistribution of moisture. These assumptions can influence the timing at which near-surface wetting signals are propagated into the modeled root zone, particularly in snow-dominated, high-elevation environments. Second, uncertainties related to VIC reflect its own structural and parameterization choices, including a three-layer soil column with spatially variable soil depth and distinct representations of vertical fluxes and subsurface drainage. These structural differences affect how surface moisture variability propagates into deeper layers and should be considered when interpreting differences in VIC and SMAP root-zone *SM* estimates.

To understand differences in root-zone *SM* timing between SMAP and VIC, *TWSA* data from GRACE were used as an independent test of the terrestrial water storage dynamics. Fig. 4a shows that VIC-derived water storage changes ($\Delta S/\Delta t = P - ET - Q$) exhibit strong temporal correspondence with GRACE from 2002 to 2024 (entire monthly time series), with R^2 = 0.86 (0.66) for the UCRB (LCRB). Multi-year average monthly water balance components further confirmed the consistent phase and amplitude of VIC and GRACE (Fig. 4b). Specifically, VIC reproduces GRACE patterns of water storage accumulation ($\Delta S/\Delta t > 0$) during the cool season, with peak accumulation rates of >2 cm mon.$^{-1}$ during December–January. Subsequently, water storage is depleted during the warm season ($\Delta S/\Delta t < 0$, April–September) due to elevated *ET* and *Q*, with maximum depletion rates of >4 cm mon.$^{-1}$ in May–June. The temporal match in both magnitude and timing illustrates that terrestrial water storage dynamics in the CRB was reproduced well by the model. This is consistent with the VIC performance in matching the long-term *Q* at sub-basin outlets (Fig. 2a–c). Despite lacking an explicit groundwater component, the three-layer soil configuration in VIC effectively simulates changes in *TWSA* below the nominal vadose zone, potentially capturing groundwater processes leading to baseflow[51]. This suggest that discrepancies in root-zone *SM* between VIC and SMAP reflect the soil parameterizations rather than fundamental deficiencies in the representation of basin-scale water storage dynamics.

To evaluate model skill in tracking interannual variability, the fall season (October–December) water storage changes, an important factor affecting spring streamflow efficiency[7], was compared between GRACE and VIC (Fig. 4c). In the UCRB, the two products have moderate positive correlation ($CC = 0.71$, Table S1), with GRACE ranging from +2.32 (2004) to −1.22 (2020) and VIC spanning from +2.52 to −1.68. As a result, VIC can track fall season water storage anomalies for years with drier or wetter initial soil moisture conditions. Wet years, including 2004, 2010, and 2016, are consistently captured by both datasets with positive anomalies, while the 2011, 2012, and 2020 drought years exhibit concordant negative anomalies. VIC occasionally misrepresents transitional hydrologic conditions, exemplified by 2009 when GRACE indicated anomalously wet conditions ($z = +0.66$) while VIC simulated anomalously wet conditions ($z =$ -0.62). Additionally, in 2006, VIC produced a wet anomaly ($z = +0.53$) not corroborated by GRACE ($z =$ -0.60). Agreement between VIC and GRACE strengthens in the LCRB, achieving a high correlation ($CC = 0.91$). These results confirm that VIC reproduces the timing and magnitude of interannual changes observed by GRACE. Remaining discrepancies likely reflect a combination of model structural limitations and uncertainties in GRACE-derived estimates. Data assimilation frameworks provide a potential pathway to reduce such differences by optimally combining model simulations with observations while explicitly accounting for uncertainties in both sources[52–53]. At the same time, GRACE-derived estimates are subject

to measurement noise, spatial leakage, and uncertainty in the attribution of individual storage components, and should be interpreted as independent, large-scale benchmarks rather than a definitive reference for model evaluation.

Discussion. This study advances previous VIC applications in the CRB by moving beyond streamflow-only calibration toward a multi-source evaluation of spatially distributed hydrologic processes and water storage dynamics using remote sensing datasets. While streamflow observations remain essential for constraining basin-integrated runoff, this study provides insight into internal model behavior that cannot be inferred from streamflow alone. The results show that VIC reproduces the timing and spatial patterns of key hydrologic states across the CRB, highlighting the complementary roles of in-situ streamflow data for calibration and satellite observations for diagnosing model process representation across space and time. Importantly, model performance exhibits systematic elevation dependence: in regions below 2,000 m, VIC and SMAP show strong temporal agreement in surface and root-zone soil moisture ($CC > 0.7$), while performance decreases at higher elevations due to the temporal phase offset discussed above (Figs. 3c–d, S2, S3). These patterns reflect the increasing complexity of snow-soil moisture interactions at higher elevations, where uncertainties in meteorological forcings (e.g., precipitation phase partitioning and temperature lapse rates) and model parameterization (e.g., snow albedo decay) exert a greater influence.

Forested high-elevation areas introduce additional complexity through canopy interception and sublimation processes that affect *SWE* accumulation and soil moisture recharge timing. These findings indicate that future improvements should prioritize high-elevation, snow-dominated regions where meteorological forcing and model parameterization uncertainties are largest. More broadly, this work demonstrates the value of using Earth observations as independent benchmarks to evaluate large-scale hydrologic models applied to the CRB. The framework presented here provides a pathway for systematically assessing where and why model performance varies across regions and processes, thereby informing future model development, calibration strategies, and potential data assimilation efforts. In this sense, the study contributes not only an updated VIC application for the CRB, but also a transferable evaluation approach that strengthens confidence in hydrologic model use for drought assessment, seasonal forecasting, and long-term water resources planning.

While the VIC model reproduces the dominant hydrologic features of the CRB, several limitations remain. Some parameters controlling snow, soil, and vegetation processes continue to be semi-calibrated at the sub-basin scale, rather than directly constrained by Earth observations. In addition, structural simplifications including the absence of an explicit groundwater component and unresolved subsurface processes, particularly lateral groundwater flow and deep percolation below the modeled soil column, may affect the partitioning of water storage changes. Furthermore,

VIC does not account for glacier mass balance, despite the contribution of glacial melt to late-summer streamflow in the headwaters of the Upper Colorado and Green sub-basins[54,55]. Advancing beyond these limitations requires a tighter integration of Earth observation datasets into model development, as well as expanding the modeling system to include physical processes that are oversimplified or missing. Beyond process enhancements, a testbed framework for systematic benchmarking of model simulations against multiple independent datasets, including SMAP, GRACE, and future Earth observation datasets, would help to facilitate the translation of scientific advances into operational tools. Such a framework would position VIC not only as a research model but also as a platform capable of bridging innovation with stakeholder needs for water resources forecasting and planning in the CRB[56].

Several sources of uncertainty should be acknowledged when interpreting these results. SMAP root-zone soil moisture is derived through model-based assimilation rather than direct observation and GRACE-derived *TWSA* is subject to measurement noise, spatial leakage, and signal attenuation from mascon processing. Combined with the model structural limitations noted above, these observational uncertainties propagate into the evaluation diagnostics presented here. Additionally, accurate *ET* estimation over dryland environments remains challenging due to strong soil water constraints, introducing uncertainty in the dominant water loss term of the CRB water budget[75]. These uncertainties have implications for

seasonal streamflow forecasting, where the high-elevation root-zone phase offset may affect spring runoff predictions, and for drought management and climate adaptation planning, where uncertainties in ET and subsurface storage propagate into estimates of long-term water availability. Reducing these uncertainties through expanded observational constraints and data assimilation remains a priority for model-based decision support in the CRB.

Methods and Datasets

The Colorado River Basin. The CRB drains approximately 630,000 km^2 across seven U.S. states and northwestern Mexico (Fig. 1a). Under the 1922 Colorado River Compact, the basin is administratively divided at Lees Ferry, Arizona, into the UCRB (Upper Basin) and Lower Colorado River Basin (LCRB or Lower Basin). The study basin exhibits elevations ranging 300 m in the arid plains of the Sonoran Desert to peaks above 4,300 m in the Rocky Mountains. This topographic variability generates hydroclimatic gradients, with mean annual precipitation varying from <100 mm yr^{-1} in Lower Basin to >1,000 mm yr^{-1} in high-elevation source areas[27]. The UCRB, despite occupying only ~35% of basin area, contributes about 92% of the natural streamflow, reflecting the dominance of snowmelt-driven hydrology in the basin water budget.

Variable Infiltration Capacity (VIC) Model and Forcing Datasets. The VIC model version 5.1 was employed (Fig. 1b)[57,58]. VIC is a macroscale land surface model that solves the water and energy balances at each computational grid cell, where each cell is divided into land cover tiles atop a three-layer soil column[59]. The uppermost soil layer (layer 1) is commonly set to a depth of 10 cm and represents surface soil moisture and fast hydrologic responses. The depths of the second and third soil layers are spatially variable and are treated as calibration parameters, controlling root-zone water availability, vertical soil moisture redistribution, and subsurface storage that contributes to baseflow[60]. VIC does not explicitly

simulate a groundwater aquifer; groundwater-related processes are represented implicitly through soil moisture dynamics and baseflow generation in the deepest soil layer. The model depicts sub-grid spatial heterogeneity through multiple land cover tiles, elevation bands, and a variable infiltration curve that parameterizes the distribution of soil moisture storage capacity[60]. The total streamflow (Q) from each grid cell is the sum of runoff (surface layer) and baseflow (third layer). VIC simulations were conducted from 1984 to 2023 at 1/16° spatial resolution (~6 km grid spacing), representing an improvement from the 1/8° resolution (~12 km) used in the USBR CRB study[61].

Meteorological forcings were updated to the Parameter-elevation Regressions on Independent Slopes Model (PRISM) dataset[62], necessitated by the discontinuation of a previously-applied gridded product beyond 2018[26,63] and its known cold biases in high-elevation areas due to a fixed lapse rate[64,65]. PRISM provides daily precipitation and minimum and maximum air temperatures at 4-km resolution using a topographically informed interpolation framework that resolves orographic precipitation gradients and regional variability[66]. PRISM fields were bilinearly interpolated to match the VIC computational grid. Additional forcing variables, including surface pressure, specific humidity, and downward shortwave and longwave radiation, were derived from the PRISM fields using MetSim[67,68]. Wind speed was obtained from Phase 2 of the North American Land Data Assimilation System (NLDAS-2)[69]. Monthly land

surface properties, including leaf area index, canopy fraction, and albedo, were derived from a 17-year climatology of MODIS observations using the MOD-LSP product, which provides spatially explicit mean seasonal cycles of these properties stratified by land cover types[23,24].

Ground and remotely-sensed datasets. We applied a combination of ground-based *SWE* and *Q*, remotely-sensed *SM*, and satellite-derived *TWSA* to independently evaluate the VIC model for key hydrologic components and spatial domains in the CRB. Naturalized streamflow and ground-based *SWE* observations were used for model calibration, while satellite-based *SM* (SMAP) and terrestrial water storage anomalies (GRACE/GRACE-FO) datasets were used for independent model evaluation. Ground observations of *SWE* were obtained from 163 Snow Telemetry (SNOTEL) stations selected based on their completeness and elevation proximity to corresponding VIC cells. The naturalized streamflow records were obtained from USBR in key sub-basins following previous studies[27]. *SM* data were obtained from the NASA SMAP Level-4 Surface and Root-Zone Soil Moisture product (L4_SM version 7)[37,70]. The SMAP satellite is directly sensitive to near-surface soil moisture, while root-zone (0–100 cm) soil moisture estimates are derived through assimilation of SMAP surface observations into CLSM using an ensemble Kalman filter. The resulting product provides globally complete estimates of surface (0–5 cm) and root-zone (0–100 cm) volumetric *SM* at 9-km, 3-hourly resolution starting from 2015. The product meets the accuracy requirement for basin-scale

hydrologic analyses, with unbiased Root Mean Squared Error (ubRMSE) ≤ 0.04 m^3/m^3. To account for systematic differences in absolute magnitudes between VIC and SMAP, *SM* values were converted to standardized anomalies (*z*-scores) absolute values over the comparison period (2015–2024). This transformation removes mean biases and focuses comparison on the relative temporal variability and spatial patterns of *SM* anomalies[71]. *TWSA* observations were obtained from the GRACE mission (2002–2017) and its successor GRACE Follow-On (2018–present)[72]. GRACE/GRACE-Follow-On satellites measure temporal variations in Earth's gravitational field caused by mass redistribution, enabling estimation of vertically integrated water storage changes including snow, surface water, soil moisture, and groundwater components. Monthly *TWSA* data were obtained from the JPL RL06 Mascon solution, which is distributed on a 0.5° grid but represents 3° equal-area caps (i.e., the effective resolution). To account for signal attenuation and leakage resulting from regularization, prior constraints, and noise suppression in the JPL RL06 mascon processing, a gain factor-based scaling approach was applied[52]. Gain factors were computed by comparing basin-averaged GRACE *TWSA* with basin-averaged Community Land Model simulated water storage anomalies. Finally, GRACE *TWSA* was compared with VIC outputs using the water balance residual approach[38] ($P - ET - Q$).

Hydrologic model calibration and evaluation. Model calibration was conducted using a manual, two-stage approach, first targeting snow

processes and then streamflow generation. Calibration was performed at the sub-basin scale using ground observations, with initial parameter values obtained from a recent VIC application in the CRB[57]. *SWE* observations from SNOTEL stations were used to guide snow process calibration, while naturalized monthly streamflow (*Q*) at sub-basin outlets was used to calibrate soil parameters. Naturalized streamflow data was produced by USBR (see https://www.usbr.gov/lc/region/g4000/NaturalFlow for details). We used naturalized streamflow records from five stations in CRB, with the gauge number and associated subbasin shown in Table S2 and Fig. S1.

Snow accumulation and ablation dynamics were calibrated by adjusting parameters governing snow surface albedo evolution and surface roughness to improve agreement with observed *SWE* from SNOTEL stations. Specifically, since PRISM corrects the cold bias present in the previous forcing product at high elevations[73], the warmer and more realistic temperature profiles required parameter adjustments to maintain accurate representation of snowpack processes. The snow albedo decay function in VIC follows:

$$\alpha_{snow} = \alpha_{max} A^{t^B}, \qquad (1)$$

where α_{max} is the albedo value of fresh fallen snow, t is the number of days since the last snowfall, and A and B are parameters set to 0.94 and 0.58 (0.82 and 0.46), respectively, during accumulation (ablation) phase. To improve the model performance, the parameters were tuned for both the accumulation (A = 0.98 and B = 0.58) and ablation phases (A = 0.92 and B

= 0.85). The parameter adjustments resulted in higher albedo values during both snow phases (Fig. S4), which reduced the snowmelt rate and improved the match with SNOTEL *SWE*. We further calibrated snow roughness (r) at a sub-basin scale to account for regional differences in snow cover. The role of r is defined within the snow energy-balance formulation of VIC[74]. Parameter adjustments effectively mitigated the underestimation of *SWE*, resulting in the accurate representation of snow dynamics, particularly in high-elevation bands (Fig. S5). The resulting parameter values for each sub-basin are summarized in Table S3.

Following snow calibration, soil parameters governing infiltration and baseflow generation were calibrated to match naturalized streamflow at sub-basin outlets. Streamflow calibration was performed at five major sub-basin outlet stations across the CRB, including the Green, Upper Colorado, San Juan, the aggregated UCRB, and the CRB above Imperial Dam (Table S2; Fig. S1). The calibration and detailed analysis focus on the UCRB because it contributes most of the naturalized inflow to Lake Powell whose reservoir levels are central to basin-wide water management. Model performance during calibration was assessed using a combined objective function consisting of the NSE for monthly Q and percent bias in annual streamflow volume. The calibration period (1984–2000) was selected to provide a multi-decadal baseline with continuous naturalized streamflow records across sub-basins, while the validation period (2001–2020) represents an independent test that includes pronounced drought

conditions and increased hydroclimatic variability. Calibrated parameters included: (1) the infiltration shape parameter (b_{inf}), which controls the variable infiltration curve representing the distribution of storage capacity; (2) the thickness of the second soil layer (D_2), affecting total column water holding capacity; (3) the maximum baseflow rate (D_{smax}, mm day^{-1}); and (4) the baseflow exponent (D_s), controlling the nonlinear relation between soil moisture in the third layer and baseflow generation. The final calibrated parameters are summarized in Table S3, and comparisons between VIC simulations and naturalized streamflow records are shown in Fig. S6. Calibration led to substantial improvements in the Green sub-basin, with monthly NSE increasing from 0.54 to 0.91, whereas improvements in the Upper Colorado sub-basin were more modest (from 0.89 to 0.91). At the scale of the aggregated UCRB, monthly streamflow performance improved from an NSE of 0.80 to 0.93. Streamflow performance at the CRB above Imperial Dam gauge, which includes the LCRB with the exception of the Gila sub-basin, is similar, as more than 90% of naturalized streamflow originates from the UCRB. The Gila sub-basin was not included due to the lack of consistent naturalized streamflow records.

Data Availability Statement. VIC and MetSim source codes are available on GitHub (https://github.com/UW-Hydro/VIC and https://github.com/UW-Hydro/MetSim, respectively). The historical meteorological forcing data are available from https://prism.oregonstate.edu. Updated VIC parameters for the CRB and

model outputs for the baseline CRB simulations conducted here are available through Zenodo (https://doi.org/10.5281/zenodo.17575686 and https://zenodo.org/uploads/17576157, respectively).

Funding Declaration. This work was supported by the NASA Applied Sciences program (Award No. 80NSSC22K0925; “Managing the Colorado River as an Infrastructure Asset: Fusing Remote Sensing and Numerical Modeling in the Operations of the Central Arizona Project”). Additional support was provided by the Arizona Water Innovation Initiative (AWII), a multi-year partnership with the State of Arizona led by Arizona State University’s Julie Ann Wrigley Global Futures Laboratory in collaboration with the Ira A. Fulton Schools of Engineering.

Acknowledgements. We appreciate the conversations with staff members of the Central Arizona Project (CAP), including Vineetha Kartha, Nolie Templeton, Orestes Morfin, and Joshua Randall. The authors also acknowledge the use of Research Computing resources at Arizona State University and would like to thank their staff for their support.

Author Contributions. Z.W. and E.R.V. conceived the ideas of the experiment. S.G. helped with data generation and organization. Z.W. generated the figures. Z.W. wrote the manuscript with important contributions from S.G. and E.R.V. All authors revised the manuscript text and made contributions to the development of the VIC application in the Colorado River Basin.

Competing Interests. The authors declare no competing interests.

References

1. U.S. Bureau of Reclamation. *Colorado River Basin Water Supply and Demand Study.* U.S. Department of the Interior Study Report, 99 pp. Available at: https://www.usbr.gov/lc/region/programs/crbstudy/finalreport/Study%20Report/StudyReport_FINAL_Dec2012.pdf (2012).
2. Udall, B. & Overpeck, J. The twenty-first century Colorado River hot drought and implications for the future. *Water Resour. Res.* **53**, 2404–2418 (2017).
3. Mote, P. W., Li, S., Lettenmaier, D. P., Xiao, M. & Engel, R. Dramatic declines in snowpack in the western US. *Npj Clim. Atmospheric Sci.* **1**, 2 (2018).
4. Milly, P. C. D. & Dunne, K. A. Colorado River flow dwindles as warming-driven loss of reflective snow energizes evaporation. *Science* **367**, 1252–1255 (2020).
5. Bass, B., Goldenson, N., Rahimi, S. & Hall, A. Aridification of Colorado River Basin's snowpack regions has driven water losses despite ameliorating effects of vegetation. *Water Resour. Res.* **59**, e2022WR033454 (2023).
6. Castle, S. L. *et al.* Groundwater depletion during drought threatens future water security of the Colorado River Basin. *Geophys. Res. Lett.* **41**, 5904–5911 (2014).

7. Tang, C. & Piechota, T. C. Spatial and temporal soil moisture and drought variability in the Upper Colorado River Basin. *J. Hydrol.* **379**, 122–135 (2009).
8. Brooks, P. D. *et al.* Groundwater dominates snowmelt runoff and controls streamflow efficiency in the western United States. *Commun. Earth Environ.* **6**, 341 (2025).
9. Rajagopalan, B. *et al.* Water supply risk on the Colorado River: Can management mitigate? *Water Resour. Res.* **45**, 1–7 (2009).
10. Reclamation, B. Reclamation announces 2022 operating conditions for Lake Powell and Lake Mead. *Newsroom* https://www.usbr.gov/newsroom/news-release/3950.
11. Wheeler, K. G. *et al.* What will it take to stabilize the Colorado River? *Science* **377**, 373–375 (2022).
12. Wang, B., Bass, B., Hall, A., Rahimi, S. & Huang, L. Disentangling climate and policy uncertainties for the Colorado River post-2026 operations. *Nat. Commun.* **16**, 8625 (2025).
13. Scanlon, B. R. *et al.* Multidecadal drought impacts on the Lower Colorado Basin with implications for future management. *Commun. Earth Environ.* **6**, 214 (2025).
14. Harding, B. L., Wood, A. W. & Prairie, J. R. The implications of climate change scenario selection for future streamflow projection in the Upper Colorado River Basin. *Hydrol. Earth Syst. Sci.* **16**, 3989–4007 (2012).

15. Lukas, J. & Payton, E. *Colorado River Basin Climate and Hydrology: State of the Science*. Western Water Assessment, University of Colorado Boulder, 531 pp. Available at: https://wwa.colorado.edu/resources/colorado-river-resources/CRBreport (2020).

16. Bennett, K. E. *et al.* Global sensitivity of simulated water balance indicators under future climate change in the Colorado Basin. *Water Resour. Res.* **54**, 132–149 (2018).

17. Vano, J. A., Das, T. & Lettenmaier, D. P. Hydrologic sensitivities of Colorado River runoff to changes in precipitation and temperature. *J. Hydrometeorol.* **13**, 932–949 (2012).

18. Vano, J. A. & Lettenmaier, D. P. A sensitivity-based approach to evaluating future changes in Colorado River discharge. *Clim. Change* **122**, 621–634 (2014).

19. Yue, H., Mascaro, G., Wang, Z., & Vivoni, E.R. Hydrometeorological forecast skill of the North American Multi-Model Ensemble in the Upper Colorado River Basin. *J. Hydrometeorol.* **26**, 933–949 (2025).

20. Xiao, M., Udall, B. & Lettenmaier, D. P. On the causes of declining Colorado River streamflows. *Water Resour. Res.* **54**, 6739–6756 (2018).

21. Christensen, N. S., Wood, A. W., Voisin, N., Lettenmaier, D. P. & Palmer, R. N. The effects of climate change on the hydrology and water resources of the Colorado River basin. *Clim. Change* **62**, 337–363 (2004).

22. Bohn, T. J., Whitney, K. M., Mascaro, G. & Vivoni, E. R. A deterministic approach for approximating the diurnal cycle of precipitation for use in large-scale hydrological modeling. *J. Hydrometeorol.* **20**, 297–317 (2019).

23. Bohn, T. J. & Vivoni, E. R. Process-based characterization of evapotranspiration sources over the North American monsoon region. *Water Resour. Res.* **52**, 358–384 (2016).

24. Bohn, T. J. & Vivoni, E. R. MOD-LSP, MODIS-based parameters for hydrologic modeling of North American land cover change. *Sci. Data* **6**, 144 (2019).

25. Andreadis, K. M., Storck, P. & Lettenmaier, D. P. Modeling snow accumulation and ablation processes in forested environments. *Water Resour. Res.* **45**, 1–13 (2009).

26. Livneh, B. *et al.* A spatially comprehensive, hydrometeorological data set for Mexico, the U.S., and Southern Canada 1950-2013. *Sci. Data* **2**, 150042 (2015).

27. Whitney, K. M. *et al.* Spatial attribution of declining Colorado River streamflow under future warming. *J. Hydrol.* **617**, (2023).

28. Wang, Z., Vivoni, E. R., Bohn, T. J. & Wang, Z. H. A multiyear assessment of irrigation cooling capacity in agricultural and urban settings of central Arizona. *J. Am. Water Resour. Assoc.* **57**, 771–788 (2021).

29. Xiang, T., Vivoni, E. R. & Gochis, D. J. Seasonal evolution of ecohydrological controls on land surface temperature over complex terrain. *Water Resour. Res.* **50**, 3852–3874 (2014).

30. Ko, A., Mascaro, G. & Vivoni, E. R. Strategies to improve and evaluate physics-based hyperresolution hydrologic simulations at regional basin scales. *Water Resour. Res.* **55**, 1129–1152 (2019).

31. Dembélé, M., Hrachowitz, M., Savenije, H. H. G., Mariéthoz, G. & Schaefli, B. Improving the predictive skill of a distributed hydrological model by calibration on spatial patterns with multiple satellite data sets. *Water Resour. Res.* **56**, e2019WR026085 (2020).

32. Koch, J., Jensen, K. H. & Stisen, S. Toward a true spatial model evaluation in distributed hydrological modeling: Kappa statistics, Fuzzy theory, and EOF-analysis benchmarked by the human perception and evaluated against a modeling case study. *Water Resour. Res.* **51**, 1225–1246 (2015).

33. Xiao, M., Mascaro, G., Wang, Z., Whitney, K. M. & Vivoni, E. R. On the value of satellite remote sensing to reduce uncertainties of regional simulations of the Colorado River. *Hydrol. Earth Syst. Sci.* **26**, 5627–5646 (2022).

34. Entekhabi, D. Propagation in the drought cascade: Observational analysis over the continental US. *Water Resour. Res.* **59**, e2022WR032608 (2023).

35. Hoylman, Z. H. *et al.* Optimizing drought assessment for soil moisture deficits. *Water Resour. Res.* **60**, e2023WR036087 (2024).

36. Reichle, R. H. *et al.* Assessment of the SMAP Level-4 surface and root-zone soil moisture product using in situ measurements. *J. Hydrometeorol.* **18**, 2621–2645 (2017).

37. Entekhabi, D. *et al.* The soil moisture active passive (SMAP) mission. *Proc. IEEE* **98**, 704–716 (2010).

38. Abdelmohsen, K., Famiglietti, J. S., Ao, Y. Z., Mohajer, B. & Chandanpurkar, H. A. Declining freshwater availability in the Colorado River Basin threatens sustainability of its critical groundwater supplies. *Geophys. Res. Lett.* **52**, e2025GL115593 (2025).

39. Scanlon, B. R. *et al.* Hydrologic implications of GRACE satellite data in the Colorado River Basin. *Water Resour. Res.* **51**, 9891–9903 (2015).

40. Bai, P., Liu, X. & Liu, C. Improving hydrological simulations by incorporating GRACE data for model calibration. *J. Hydrol.* **557**, 291–304 (2018).

41. Zhang, L. *et al.* Validation of terrestrial water storage variations as simulated by different global numerical models with GRACE satellite observations. *Hydrol. Earth Syst. Sci.* **21**, 821–837 (2017).

42. Hale, K. E., Musselman, K. N., Newman, A. J., Livneh, B. & Molotch, N. P. Effects of snow water storage on hydrologic partitioning across the mountainous, western United States. *Water Resour. Res.* **59**, e2023WR034690 (2023).

43. Han, J. *et al.* Streamflow seasonality in a snow-dwindling world. *Nature.* **629**, 1075–1081 (2024).

44. Carroll, R. W. H., Gochis, D. & Williams, K. H. Efficiency of the summer monsoon in generating streamflow within a snow-dominated headwater basin of the Colorado River. *Geophys. Res. Lett.* **47**, e2020GL090856 (2020).

45. Wang, Z., Jaya Baskar, J. V., Sistla Naga Sai, M. S., Svoma, B. & Vivoni, E. R. Spatiotemporal patterns of intermittent snow cover from PlanetScope imagery using deep learning. *Geophys. Res. Lett.* **52**, e2025GL116582 (2025).

46. Trujillo, E. & Molotch, N. P. Snowpack regimes of the western United States. *Water Resour. Res.* **50**, 5611–5623 (2014).

47. Mascaro, G., Ko, A. & Vivoni, E. R. Closing the loop of satellite soil moisture estimation via scale invariance of hydrologic simulations. *Sci. Rep.* **9**, 16123 (2019).

48. Vivoni, E. R. *et al.* Observed relation between evapotranspiration and soil moisture in the North American monsoon region. *Geophys. Res. Lett.* **35**, L22403 (2008).

49. Bateni, S. M. & Entekhabi, D. Relative efficiency of land surface energy balance components. *Water Resour. Res.* **48**, W04510 (2012).

50. Koster, R. D., et al. A catchment-based approach to modeling land surface processes in a general circulation model: 1. Model structure. *J. Geophys. Res. Atmos.* **105**, 809–824 (2000).

51. Getirana, A., Kumar, S. & Rodell, M. Inconsistencies in GRACE-based groundwater storage estimation—A call for a proper use of land surface models. *Geophys. Res. Lett.* **52**, e2025GL119197 (2025).
52. Kumar, S. *et al.* An agenda for land data assimilation priorities: Realizing the promise of terrestrial water, energy, and vegetation observations from space. *J. Adv. Model. Earth Syst.* **14**, e2022MS003259 (2022).
53. Nie, W. *et al.* Assimilating GRACE into a land surface model in the presence of an irrigation-induced groundwater trend. *Water Resour. Res.* **55**, 11274–11294 (2019).
54. Boardman, E. N. Constraining kilometer-scale mountain snow transport and snowshed areas. *Geophys. Res. Lett.* **52**, e2024GL113599 (2025).
55. Boardman, E. N. *et al.* Wind and topography underlie correlation between seasonal snowpack, mountain glaciers, and late-summer streamflow. *The Cryosphere* **19**, 3193–3225 (2025).
56. Whitney, K. M. *et al.* A stakeholder-engaged approach to anticipating forest disturbance impacts in the Colorado River Basin under climate change. *J. Water Resour. Plan. Manag.* **149**, 04023020 (2023).
57. Wang, Z., Vivoni, E. R., Whitney, K. M., Xiao, M. & Mascaro, G. On the sensitivity of future hydrology in the Colorado River to the selection of the precipitation partitioning method. *Water Resour. Res.* **60**, e2023WR035801 (2024).
58. Hamman, J. J., Nijssen, B., Bohn, T. J., Gergel, D. R. & Mao, Y. The variable infiltration capacity model version 5 (VIC-5): Infrastructure

improvements for new applications and reproducibility. *Geosci. Model Dev.* **11**, 3481–3496 (2018).

59. Liang, X., Wood, E. F. & Lettenmaier, D. P. Surface soil moisture parameterization of the VIC-2L model: Evaluation and modification. *Glob. Planet. Change* **13**, 195–206 (1996).

60. Liang, X., Lettenmaier, D. P., Wood, E. F. & Burges, S. J. A simple hydrologically based model of land surface water and energy fluxes for general circulation models. *J. Geophys. Res.* **99**, 14415 (1994).

61. U.S. Bureau of Reclamation. *Colorado River Basin Water Supply and Demand Study, Technical Report B – Water Supply Assessment, Appendix B4: Variable Infiltration Capacity (VIC) Hydrologic Modeling Methods and Simulations,* 18 pp. Available at: https://www.usbr.gov/lc/region/programs/crbstudy/finalreport/Technical%20Report%20B%20-%20Water%20Supply%20Assessment/TR-B_Appendix4_FINAL.pdf (2012).

62. Daly, C., Neilson, R. P. & Phillips, D. L. A statistical-topographic model for mapping climatological precipitation over mountainous terrain. *J. Applied Meteorol. Climatol*. **33**, 140–158 (1994).

63. Su, L. *et al.* Drought variability over the conterminous United States for the past century. *J. Hydrometeorol.* **22**, 1153–1168 (2021).

64. Walton, D. & Hall, A. An assessment of high-resolution gridded temperature datasets over California. *J. Clim.* **31**, 3789–3810 (2018).

65. Whitney, K. M. *et al.* Quantifying the impacts of dynamic lapse regimes on snow simulations over complex terrains. *J. Hydrometeorol.* **26**, 1525–1560 (2025).

66. Daly, C. *et al.* Physiographically sensitive mapping of climatological temperature and precipitation across the conterminous United States. *Int. J. Climatol.* **28**, 2031–2064 (2008).

67. Bohn, T. J. *et al.* Global evaluation of MTCLIM and related algorithms for forcing of ecological and hydrological models. *Agric. For. Meteorol.* **176**, 38–49 (2013).

68. Bennett, A., Hamman, J. & Nijssen, B. MetSim: A Python package for estimation and disaggregation of meteorological data. *J. Open Source Softw.* **5**, 2042 (2020).

69. Cosgrove, B. A., *et al.* Real-time and retrospective forcing in the North American Land Data Assimilation System (NLDAS) project. *J. Geophys. Res*, **108**(D22), 8842 (2003).

70. Reichle, R. *et al.* SMAP L4 Global 9 km EASE-Grid Surface and Root Zone Soil Moisture Geophysical Data. (SPL4SMGP, Version 7). NASA National Snow and Ice Data Center Distributed Active Archive Center. Available at: https://doi.org/10.5067/T5RUATAQREF8. (2022).

71. Koster, R. D. *et al.* On the nature of soil moisture in land surface models. *J. Clim.* **22**, 4322–4335 (2009).

72. Rodell, M. & Famiglietti, J. S. An analysis of terrestrial water storage variations in Illinois with implications for the Gravity Recovery and Climate Experiment (GRACE). *Water Resour. Res.* **37**, 1327–1339 (2001).

73. Eldardiry, H. *et al.* Characterizing how meteorological forcing selection and parameter uncertainty influence Community Land Model Version 5 hydrological applications in the United States. *J. Adv. Model. Earth Syst.* **17**, e2024MS004222 (2025).

74. Andreadis, K. M., P. Storck, & D. P. Lettenmaier. Modeling snow accumulation and ablation processes in forested environments. *Water Resour. Res*. **45**, W05429 (2009).

75. Jawad, M. *et al.* Improved evapotranspiration estimation using the Penman-Monteith equation with a deep learning (DNN) model over the dry southwestern US: Comparison with ECOSTRESS, MODIS, and OpenET. *J. Hydrol.* **660**, 133460 (2025).

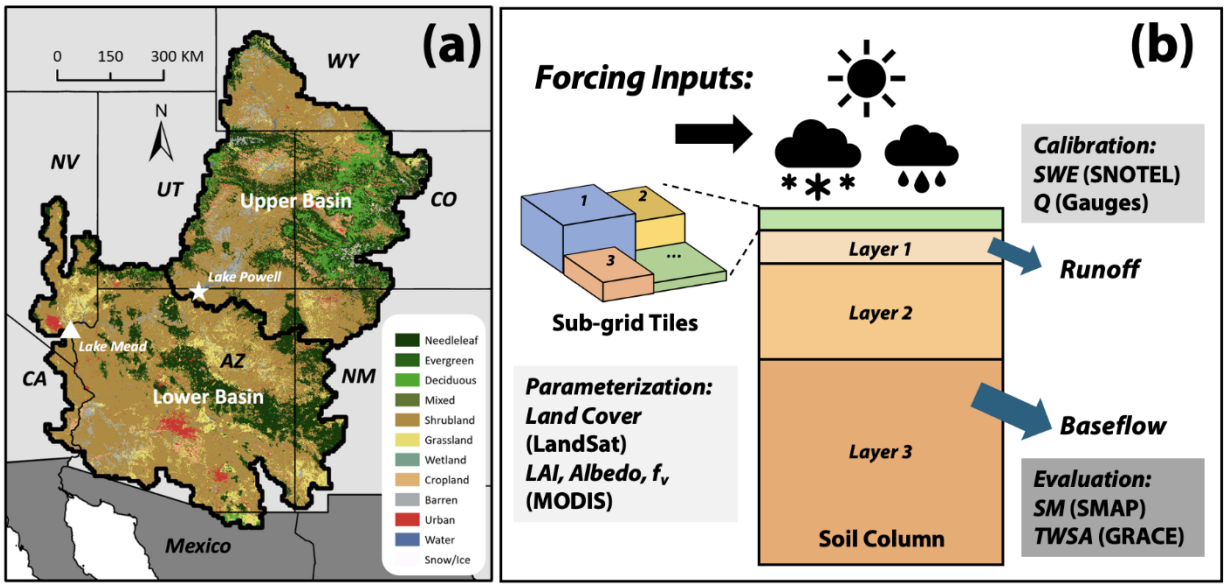

Fig. 1. Study area and conceptual diagram of the model structure. (a) Land cover map in the CRB from the National Land Cover Database 2023 (https://www.mrlc.gov) with Upper Basin and Lower Basin boundaries. (b) Conceptual diagram of VIC model structure and the Earth observation products used in this study. VIC represents hydrologic processes at the grid cell scale, with sub-grid tiles used to characterize heterogeneity in land cover types within each grid cell. Vegetation properties for each tile, including leaf area index (*LAI*), albedo, and canopy fraction (f_v), are derived from MODIS-based products. Ground-based observations of snow water equivalent (*SWE*) from Snow Telemetry (SNOTEL) stations and naturalized streamflow (*Q*) from U.S. Bureau of Reclamation (USBR) are used for model calibration. Independent evaluation datasets include soil moisture (*SM*) from the Soil Moisture Active Passive (SMAP) mission and terrestrial water storage anomalies (*TWSA*) from the Gravity Recovery and Climate Experiment (GRACE) and GRACE Follow-On missions.

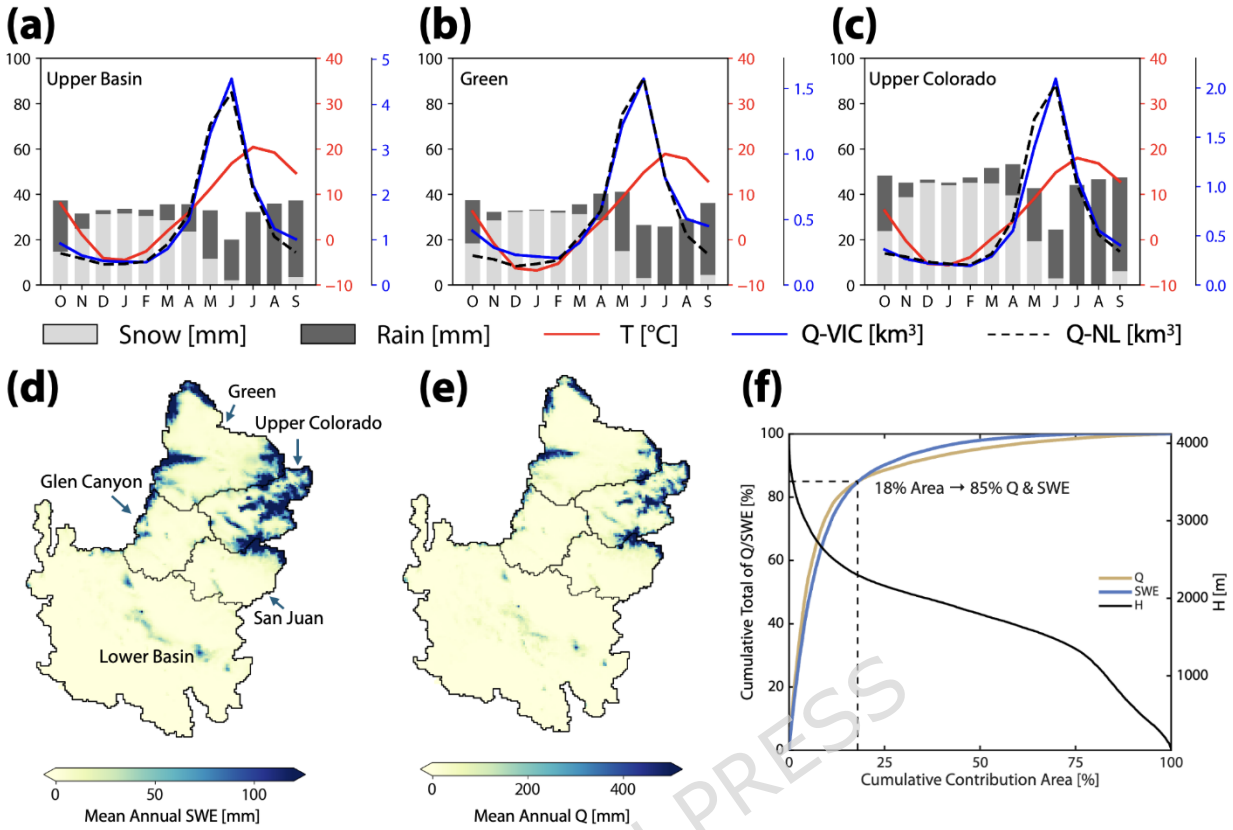

Fig. 2. Hydroclimatic characteristics of the Colorado River Basin as represented by VIC model simulations. (a) Monthly climatology (1984–2023) of total precipitation (partitioned into snow and rain, mm/mon.), averaged air temperature (T, □C), and streamflow (Q, km^3/mon.) from VIC simulations (Q-VIC, blue) and naturalized streamflow record (Q-NL, black dashed) in the UCRB (or Upper Basin). (b)-(c) Same as (a), but for Green and Upper Colorado sub-basins. (d) Spatial distribution of mean annual snow water equivalent (SWE, mm) from VIC simulations. (e) Mean annual streamflow (mm yr^{-1}) from VIC simulations. (f) Cumulative fraction of SWE and Q as a function of contributing area (A_f, %), with elevation (H, m) profile shown on the right axis.

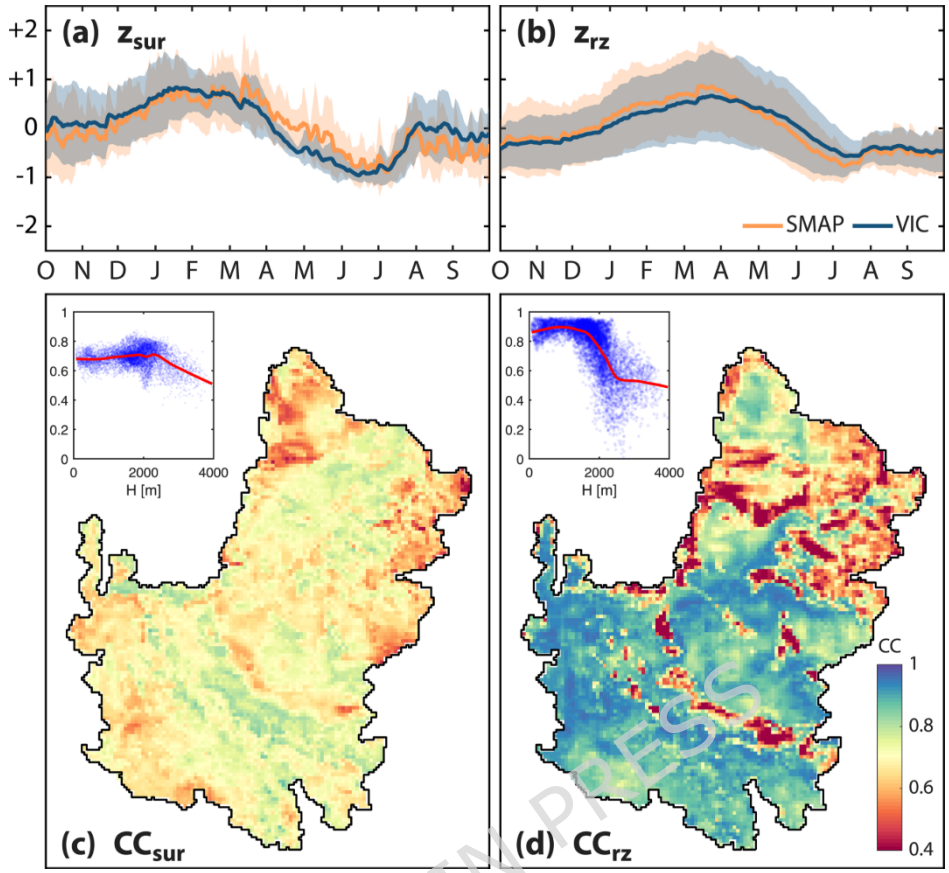

Fig. 3. Model evaluation with Earth Observation datasets. (a–b) Monthly variations of standardized anomalies of surface (a, z_{sur}) and root-zone (b, z_{rz}) soil moisture, averaged across the CRB from VIC and SMAP during the period of 2015–2024. Shading denote interannual variability, calculated as one standard deviation from the multi-year average. (c–d) Maps of temporal correlation coefficients of standardized anomalies of surface (c, CC_{sur}) and root-zone (d, CC_{rz}) soil moisture between VIC and SMAP. Insets show elevation (H, m) variation of correlation coefficients, respectively. The red lines represent the smoothened trend of the data using a LOWESS (locally weighted regression) function.

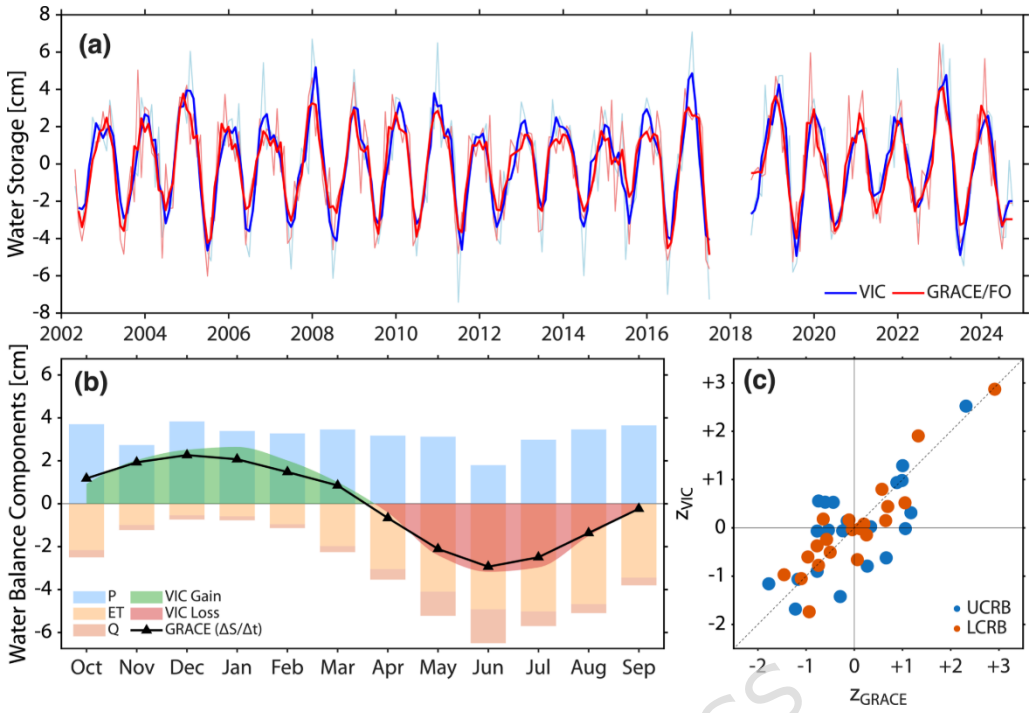

Fig. 4. Evaluation of basin-scale terrestrial water storage dynamics from VIC and GRACE. (a) Changes in terrestrial water storage from VIC and GRACE during 2002–2024 shown as monthly values (thin lines) and three-month moving average (thick lines) in the UCRB. (b) Multi-year mean monthly water balance components highlight consistent timing and magnitude of terrestrial water storage gains ($\Delta S/\Delta t > 0$, green shaded areas) and losses ($\Delta S/\Delta t < 0$, red shaded areas) in VIC as compared to GRACE *TWSA* (labelled GRACE $\Delta S/\Delta t$, black lines with symbols) in the UCRB. (c) Scatterplot of standardized anomalies in terrestrial water storage from GRACE and VIC in the fall season (October–December) of all years in 2002–2024 averaged in the UCRB and LCRB.